21. Puin, W., Rodewald, S., Ramlau, R., Heitjans, P. & Maier, J. Local and overall ionic conductivity in nanocrystalline CaF_2. *Solid State Ionics* **131,** 159–164 (2000).
22. Schoonman, J. Nanostructured materials in solid state ionics. *Solid State Ionics* **135–137,** 5–20 (2000).
23. Tuller, H. L. Ionic conduction in nanocrystalline materials. *Solid State Ionics* **131,** 143–157 (2000).

Acknowledgements

We thank W. Kussmaul for experimental assistance, G. Bilger and H. Kerber for the performance of SIMS and X-ray pole-figure measurements, and W. Dietsche for advice.

Correspondence and requests for materials should be addressed to J.M. (e-mail: weiglein@chemix.mpi-stuttgart.mpg.de) or to U.S. (e-mail: sata@chemix.mpi-stuttgart.mpg.de).

Pairing of isolated nucleic-acid bases in the absence of the DNA backbone

Eyal Nir*, Karl Kleinermanns† & Mattanjah S. de Vries*‡

* *Department of Chemistry, The Hebrew University of Jerusalem, Jerusalem 91904, Israel*
† *Institut für Physikalische Chemie und Elektrochemie, Heinrich Heine Universität, D-40225 Düsseldorf, Germany*
‡ *Department of Chemistry and Biochemistry, University of California, Santa Barbara, California 93106, USA*

The two intertwined strands of DNA are held together through base pairing—the formation of hydrogen bonds between bases located opposite each other on the two strands. DNA replication and transcription involve the breaking and re-forming of these hydrogen bonds, but it is difficult to probe these processes directly. For example, conventional DNA spectroscopy[1–3] is dominated by solvent interactions, crystal modes and collective modes of the DNA backbone; gas-phase studies, in contrast, can in principle measure interactions between individual molecules in the absence of external effects, but require the vaporization of the interacting species without thermal degradation[4–9]. Here we report the generation of gas-phase complexes comprising paired bases, and the spectroscopic characterization of the hydrogen bonding in isolated guanine–cytosine (G–C) and guanine–guanine (G–G) base pairs. We find that the gas-phase G–C base pair adopts a single configuration, which may be Watson–Crick, whereas G–G exists in two different configurations, and we see evidence for proton transfer in the G–C pair, an important step in radiation-induced DNA damage pathways[10]. Interactions between different bases and between bases and water molecules can also be characterized by our approach, providing stringent tests for high-level *ab initio* computations that aim to elucidate the fundamental aspects of nucleotide interactions[11–13].

In order to form isolated base pairs in the gas phase we desorb a mixture of neat bases from a graphite surface using 10-ns laser pulses at 1,064 nm and at 1 mJ cm^{-2}, followed by entrainment of the neutral, non-fragmented base molecules in a supersonic expansion of argon gas[14]. The expansion lowers the internal temperature of the molecules to a few tens of degrees Kelvin and induces cluster formation. In this way we have formed over 20 different base-pair combinations. By admixing water with the drive gas we can also form clusters of the bases with water molecules, simulating the solvent environment. We have formed such clusters ranging in size from one to fifty water molecules, attached to a single base molecule. We analyse the cold base pairs or clusters downstream with resonance-enhanced multiphoton ionization (REMPI): a photon from a tunable dye laser excites the molecules to the first excited singlet state, whereas a second photon ionizes only those molecules that are excited by the first. We detect the ions in a time-of-flight mass spectrometer. By varying the wavelength we obtain a mass-selected vibronic excitation spectrum. We obtained spectra of all individual bases, of guanine clusters with a single water molecule, and of a variety of base pairs (see Supplementary Information). In order to distinguish different cluster structures we apply spectral hole burning (SHB): while one laser is tuned over all transitions, a second laser, with a 30-ns delay and tuned permanently to a single

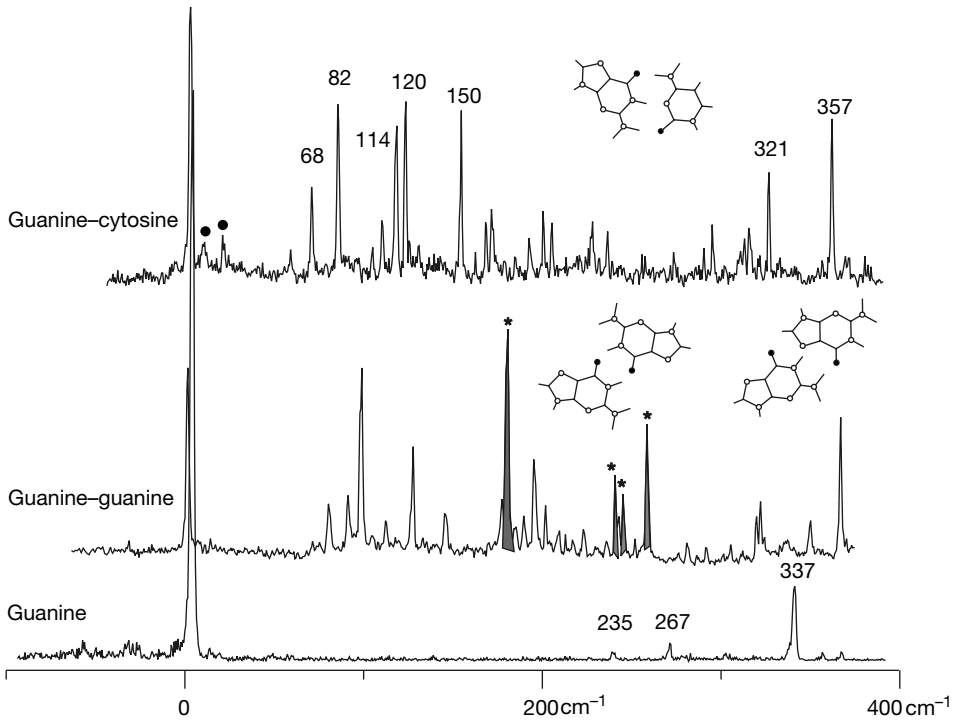

Figure 1 Resonance-enhanced multiphoton ionization (REMPI) spectrum of guanine and its dimers with guanine and cytosine. The spectra are offset such that the origins (0–0 transitions) are shown at the same position for all three species. See text for details.

transition, monitors ground-state depletion for a selected cluster species. Similarly, by using an infrared laser to deplete the ground state resonantly, we can obtain infrared spectra of selected species.

Figure 1 shows simultaneously recorded REMPI spectra for the G–C dimer, the G–G dimer and the G monomer, which are offset such that the origins (0–0 transitions) are shown at the same position. The G–C and G–G origins are blue-shifted by 446 cm^{-1} and by 235 cm^{-1}, respectively, with respect to the G origin at 32,868 cm^{-1}. Neither the G nor the C chromophore of the dimers absorbs in the first 200 wavenumbers above the origin of the complex. The guanine spectrum exhibits its first significant vibronic activity at 235 cm^{-1}, whereas cytosine absorption is strongly blue-shifted to about 36,000 cm^{-1}, as has been seen for uracil and thymine[4]. Therefore, when we excite the guanine chromophore in the G–G and G–C complexes, we can observe hydrogen bond vibrations built on the 0–0 transition without any interference. Indeed, all spectral lines in the first two hundred wavenumbers of these spectra can be assigned to hydrogen-bond vibrations.

The shaded peaks in the G–G spectrum are due to a different species, as determined by SHB, implying the presence of two different hydrogen-bonded G–G structures. In the case of G–C, SHB shows that all peaks belong to the same species; thus we observe one G–C structure only.

Table 1 summarizes the major lines for G–C. The frequencies of the less intense bands in the range 160–230 cm^{-1} all fit those of overtones and combination bands of the major lines. The bands at 321 and 357 cm^{-1} are the least energetic intramolecular G vibrations of G–C that we observed and probably correspond to in-plane ring deformations of G with symmetric and antisymmetric C–NH_2 and C=O bend motions, respectively[13]. The two low-frequency peaks in the spectrum, marked with circles, are absent when we use krypton as the drive gas instead of argon. This suggests that they may be due to hot bands or result from dissociating clusters with argon, rather than G–C vibrations.

The cluster comprised of one guanine base and one cytosine base has six intermolecular modes, reflecting the loss of three rotations and three vibrations upon complexation. We can describe the six possible modes as follows: (1) The butterfly motion, γ_s, with G and C as wings; (2) the out-of-plane torsion, τ; and (3) the in-plane bending (gearing), δ, of G and C. These three motions can be correlated with monomer rotations approximately around the free short axis, the long axis and the axis perpendicular to the plane respectively. (4) The symmetric stretch, σ_s, and (5) the antisymmetric stretch, σ_{as}. These motions correlate with translations of the monomers parallel and perpendicular to the H-bond. (6) The displacements of G and C in opposite directions perpendicular to the molecular plane (alternating stairs), γ_{as}, correlating with monomer translations perpendicular to their planes.

In recent years, high-level *ab initio* calculations on DNA base pairs have been carried out. The results of these calculations aid us with the interpretation of our spectra, but the experimental data also provide a firm benchmark for theory. In Table 1 we compare our experimental frequencies with the *ab initio* values calculated by refs 11–13 for the Watson–Crick (WC) configuration of this base pair. Agreement is particularly good for calculations at the HF/6-31G(d) and the HF/6-31G(d,p) levels, which are known to yield relatively reliable harmonic intermolecular frequencies without the need to resort to scaling factors[15,16]. Deviations due to anharmonicity should be important only for out-of-plane vibrations, the first two of which are missing in our G–C spectrum owing to their low transition strength. It seems reasonable to compare ground-state calculations and excited-state measurements, because the guanine origin intensity is an order of magnitude larger than that of its vibronic transitions, which suggests that there is little difference between the geometry of guanine in the ground, and the excited state. In order to assess the extent to which the agreement with calculations for the WC structure constitutes a unique fit, we have also calculated the vibrational frequencies for eight other structures, obtained by minimizing different starting configurations. These computations, at the HF 6-31G(d,p) level, give results for the WC structure identical to those of ref. 12 and agree rather less well with the experimental data for all other structures. Further determination for the gas-phase G–C structure will follow from infrared spectral hole burning on the G origin of the pair, for which we can observe N–H and O–H stretch frequencies, as well as their shifts upon complexation (see the Supplementary Information for IR hole burning results on the isolated G). We have also studied clusters between guanine and methyl-substituted cytosines. Clusters with 5-methylC show spectra identical to those of the unsubstituted ones, while clusters with 3-methylC show a very different spectrum. These results are also consistent with a WC structure for the unsubstituted G–C pairs. Further support for this conclusions might be derived from band-contour and isotope-shift measurements.

The REMPI spectrum of the G–G base pair likewise shows low-frequency vibrations in the range up to 200 cm^{-1}, which can again be ascribed to intermolecular vibrations and their overtones and combination bands. Spectral hole burning reveals the existence of two sets of peaks in this spectrum (distinguished by peak shading and asterisks in Fig. 1), implying two different cluster structures. *Ab initio* calculations of the G–G structure at different levels of theory agree that the structures displayed in Fig. 1 are the two most stable ones[17,18]. When both monomer parts in the dimer are identical, only one electronic spectrum is expected, whereas exciton splitting may lead to a second electronic band system. A further analysis, which awaits more detailed calculations for this base pair, should thus allow us to distinguish between the symmetric and the non-symmetric structure.

Table 1 Intermolecular vibrational frequencies of the G–C base pair in the S_1 state

Frequency* (sm^{-1})	Relative intensity†	Label	Description	*Ab initio*		
				HF/6-31G(d)‡	HF/6-31G(d,p)§	BP86/6-3111G‖
		γ_s	Symmetric out-of-plane bending (butterfly)	20	25	29
		τ	Torsion	32	34	44
67.5	0.30	γ_{as}	Antisymmetric out-of-plane bending	66	69	85
81.8	0.64	δ¶	In-plane bending	84	84	105
106.4	0.17	$\gamma_s + \delta/\gamma_{as} + \tau$				
114.4	0.54	σ_{as}¶	Antisymmetric stretching	117	116	145
119.5	0.65	σ_s	Symmetric stretching	125	123	150
150.4	0.62	$\gamma_{as} + \sigma_{as}/\sigma_s$#				

* Relative to the electronic origin at 33,313 cm^{-1}; experimental uncertainty is ±0.5 cm^{-1}.
† Relative to origin intensity.
‡ Ref. 3.
§ Ref. 4.
‖ Ref. 5.
¶ The two normal mode motions are very similar and can also be regarded as rotations of G (or C) about the axis perpendicular to their planes with the other cluster moiety, C (or G) performing an opposite, smaller-amplitude rotation to conserve the centre of mass.
# The solidus indicates alternative assignments.

Experiments using laser desorption from an equimolar mixture of guanine, adenine, cytosine, thymine and uracil yielded mass peaks for all combinations of G with the other bases and clusters comprised of two, three and four bases (see Supplementary Information). The abundance ratios depend on wavelength because ionization profiles and ionization efficiencies differ. *Ab initio* calculations at different levels of theory agree that the G–C Watson–Crick base pair with three nearly linear hydrogen bonds and the symmetrically hydrogen-bonded G–G base pair are the most stable base pairs[19]. These two base pairs indeed appear to form preferentially in our system, but we cannot derive absolute association constants because jet expansion clusters are not formed under thermal equilibrium conditions.

Proton transfer between bases in a base-pair radical cation and subsequent reactions in the nucleotides are assumed to be a major source of damage of DNA by ionizing radiation[10]. We observed the electronic origin band of G–C also as a spectral peak at the mass of $(C + H)^+ (m/e = 112)$. This implies a fast $G \rightarrow C$ proton transfer after excitation, followed by dissociation into the $(C + H)^+$ ion and either the $(G - H)$ radical or the $(G - H)^-$ negative ion. The hydrogen transfer can take place either in the S_1 excited state or in the ionic ground state. The measurements were performed at rather low laser fluence ($\sim$100 μJ, 10-ns pulse width, 2-mm beam diameter) such that absorption of a further photon by the $(G + C)^+$ ion is unlikely. The total excitation energy available from two photons at the resonant wavelength is 8.26 eV ($2 \times 33313\ cm^{-1}$). This is very close to the vertical ionization potential of guanine[20] and is probably insufficient to lead to $G^+ + C$ as products. The fact that we do observe dissociation of the ion with $(C + H)^+$ as a product channel at this energy, but that dissociation into $G^+ + C$ does not occur, suggests that proton transfer weakens the bonding in the complex ion.

We have generated gas-phase complexes comprised of selected DNA bases whose interaction can be probed free of interactions with other bases or solvent molecules. This approach allows the generation of gas-phase complexes containing a single base and water molecules as well, and the use of mass-selected detection should therefore make it possible to elucidate the influence of the solvent in detail, one water molecule at a time[21]. Finally, as the electronic ground state of water clusters is experimentally accessible by using infrared-ultraviolet double resonance spectroscopy, we expect that detailed comparisons with theoretical predictions will be possible. □

Received 27 August 1999; accepted 9 November 2000.

1. Fodor, S. P. *et al.* H/Sub 2/Raman-shifted YAG laser ultraviolet raman spectrometer operating at wavelengths down to 184 nm. *J. Raman Spectrosc.* **17,** 471–475 (1986).
2. Urabe, H. *et al.* Collective vibrational modes in molecular assembly of DNA and its application to biological systems. Low frequency raman spectroscopy. *J. Chem. Phys.* **82,** 531–535 (1985).
3. Cocco, S. & Monasson, R. Theoretical study of collective modes in DNA at ambient temperature. *J. Chem. Phys.* **112,** 10017–10033 (2000).
4. Brady, B. B., Peteanu, L. A. & Levy, D. H. The electronic spectra of the pyrimidine bases uracil and thymine in a supersonic molecular beam. *Chem. Phys. Lett.* **147,** 538–543 (1988).
5. Viant, M. R. *et al.* Infrared laser spectroscopy of uracil in a pulsed slit jet. *J. Chem. Phys.* **103,** 9502–9505 (1995).
6. Nir, E. *et al.* REMPI spectroscopy of jet cooled guanine. *J. Am. Chem. Soc.* **121,** 4896–4897 (1999).
7. Yanson, I. K., Teplitsky, A. B. & Sukhodub, L. F. Molecular interactions in nucleic acids. *Biopolymers* **18,** 1149–1170 (1997).
8. Dey, M. *et al.* Base pair formation of free nucleobases and mononucleosides in the gas phase. *J. Am. Chem. Soc.* **116,** 9211–9215 (1994).
9. Dey, M., Grotemeyer, J. & Schlag, E. W. Pair formation of free nucleobases and mononucleosides in the gas-phase. *Z. Naturforsch.* **49A,** 776–784 (1994).
10. Hutter, M. & Clark, T. On the enhanced stability of the guanine-cytosine base-pair radical cation. *J. Am. Chem. Soc.* **118,** 7574–7577 (1996).
11. Florian, J., Leszczynski, J., Johnson, B. G. On the intermolecular vibrational modes of the guanine-cytosine, adenine-thymine and formamide-formamide H-bonded dimers. *J. Mol. Struct.* **349,** 421–426 (1995).
12. Shishkin, O., Sponer, J., Hobza, P. Intermolecular flexibility of DNA bases in adenine-thymine and guanine-cytosine Watson-Crick base pairs. *J. Mol. Struct.* **477,** 15–21 (1999).
13. Santamaria, R. *et al.* Vibrational spectra of nucleic acid bases and their Watson-Crick pair complexes. *J. Comput. Chem.* **20,** 511–530 (1999).
14. Meijer, G. *et al.* Laser desorption jet-cooling of organic molecules. Cooling characteristics and detection sensitivity. *Appl. Phys. B* **51,** 395–403 (1990).
15. Schutz, M., Burgi, T. & Leutwyler, S. Intermolecular bonding and vibrations of phenol.H_2O (D_2O). *J. Chem. Phys.* **98,** 3763–3777 (1993).
16. Schmitt, M., Jacoby, C. & Kleinermanns, K. Torsional splitting of the intermolecular vibrations of phenol (H_2O)1 and its deuterated isotopomers. *J. Chem. Phys.* **108,** 4486–4495 (1997).
17. Sponer, J., Leszczynski, J. & Hobza, P. Structures and energies of hydrogen-bonded DNA base pairs. A nonempirical study with inclusion of electron correlation. *J. Phys. Chem.* **100,** 1965–1974 (1995).
18. Hobza, P. *et al.* Performance of empirical potentials (AMBER, CFF95, CVFF, CHARMM, OPLS, POLTEV), semiempirical quantum chemical methods (AM1, MNDO/M, PM3), and ab initio Hartree-Fock method for interaction of DNA bases: Comparison with nonempirical beyond Hartree-Fock results. *J. Comput. Chem.* **18,** 1136–1150 (1997).
19. Hobza, P. & Sponer, J. Thermodynamic characteristics for the formation of H-bonded DNA base pairs. *Chem. Phys. Lett.* **261,** 379–384 (1996).
20. Colson, A. *et al.* Ab initio molecular orbital calculations on DNA base pair radical ions: Effect of base pairing on proton-transfer energies, electron affinities, and ionization potentials. *J. Phys. Chem.* **96,** 9787–9794 (1992).
21. Janzen, C. *et al.* Structure and vibrations of Phenol(H_2O)7,8 studied by infrared-ultraviolet and ultraviolet-ultraviolet double-resonance spectroscopy and ab initio theory. *J. Chem. Phys.* **110,** 9898–9907 (1999).

Supplementary information is available on *Nature*'s World-Wide Web site (http://www.nature.com) or as paper copy from the London editorial office of *Nature*.

Acknowledgements

This work has been supported by the Deutsche Forschungsgemeinschaft and United States–Israel Binational Science Foundation.

Correspondence and requests for materials should be addressed to M.S.d.V. (e-mail: devries@chem.ucsb.edu).

The influence of rivers on marine boron isotopes and implications for reconstructing past ocean pH

D. Lemarchand, J. Gaillardet, É. Lewin & C. J. Allègre

Laboratoire de Géochimie et Cosmochimie, Institut de Physique du globe de Paris, 4 place Jussieu, 75252 Paris Cedex 05

Ocean pH is particularly sensitive to atmospheric carbon dioxide content[1–3]. Records of ocean pH can therefore be used to estimate past atmospheric carbon dioxide concentrations. The isotopic composition of boron ($\delta^{11}B$) contained in the carbonate shells of marine organisms varies according to pH, from which ocean pH can be reconstructed[4–11]. This requires independent estimates of the $\delta^{11}B$ of dissolved boron in sea water through time. The marine $\delta^{11}B$ budget, however, is still largely unconstrained. Here we show that, by incorporating the global flux of riverine boron (as estimated from $\delta^{11}B$ measurements in 22 of the world's main rivers), the marine boron isotope budget can be balanced. We also derive ocean $\delta^{11}B$ budgets for the past 120 Myr. Estimated isotope compositions of boron in sea water show a remarkable consistency with records of $\delta^{11}B$ in foraminiferal carbonates[9–11], suggesting that foraminifera $\delta^{11}B$ records may in part reflect changes in the marine boron isotope budget rather than changes in ocean pH over the Cenozoic era.

The present-day concentration of boron in the oceans and its isotopic composition ($\delta^{11}B_{sw}$) are both uniform, with values of 4.5 p.p.m. and +39.6‰, respectively ($\delta^{11}B$ is defined in Table 1). Although a number of previous investigations have led to the identification of the main processes affecting boron in the ocean, the oceanic cycle of boron and its secular evolution are still not known. The sinks of boron in the ocean are divided into three classes: uptake during low-temperature weathering of the oceanic crust[12,13], adsorption on clastic sediments[14,15] and coprecipitation in carbonates[4]. To balance these outputs from the oceans, three sources have been proposed: rivers, hydrothermal vents and fluid expelled